

Article

Effect of Freeze-Thaw Damage on the Physical, Mechanical, and Acoustic Behavior of Sandstone in Urumqi

Junce Xu ¹ , Hai Pu ^{1,2,*}  and Ziheng Sha ¹ 

¹ State Key Laboratory for Geomechanics & Deep Underground Engineering, China University of Mining & Technology, Xuzhou 221116, China

² Xinjiang Institute of Engineering, College of Mining Engineering and Geology, Urumqi 830091, China

* Correspondence: haipu@cumt.edu.cn

Abstract: The Urumqi area in China is a seasonally cold region, and the rock structures in the region are susceptible to freeze-thaw (F-T) weathering. Therefore, this study investigated the effect of F-T on the physical, mechanical, and fracture behavior of sandstone from Urumqi. The acoustic emission method (AE) was used to determine the stress thresholds for the initiation and development of cracks in the samples under cyclic F-T action. The results suggested that parameters such as P-wave velocity, elastic modulus, and peak stress presented a significant negative correlation with F-T damage, while porosity exhibited a close positive correlation. The elastic modulus of the sample was more sensitive to the F-T action with the smallest half-life (27 cycles) and the largest decay factor (0.0254). In addition, the stress threshold for micro-cracks development and macro-cracks initiation in the samples decreased with increasing F-T damage. After 30 F-T cycles, the stress threshold for micro-cracks propagation in the samples decreased from 20.73 MPa to 5.02 MPa by approximately 76%. The normalized stress threshold for the macro-cracks initiation was also decreased from 0.93 to 0.71. Moreover, the macro-cracks damage zone of the samples showed an increasing trend with F-T damage, from 7% under natural conditions to 29% after 30 cycles. It is concluded that F-T action lowers the stress thresholds for cracks development in sandstone in the Urumqi area, posing serious safety concerns for mass rock engineering in this area.

Keywords: mechanical properties; acoustic emission; freeze-thaw damage; stress threshold



Citation: Xu, J.; Pu, H.; Sha, Z. Effect of Freeze-Thaw Damage on the Physical, Mechanical, and Acoustic Behavior of Sandstone in Urumqi. *Appl. Sci.* **2022**, *12*, 7870. <https://doi.org/10.3390/app12157870>

Academic Editor: Stefano Invernizzi

Received: 13 July 2022

Accepted: 4 August 2022

Published: 5 August 2022

Publisher's Note: MDPI stays neutral with regard to jurisdictional claims in published maps and institutional affiliations.



Copyright: © 2022 by the authors. Licensee MDPI, Basel, Switzerland. This article is an open access article distributed under the terms and conditions of the Creative Commons Attribution (CC BY) license (<https://creativecommons.org/licenses/by/4.0/>).

1. Introduction

The geomechanical behavior of rocks under freeze-thaw (F-T) action has drawn considerable attention due to its crucial role in many rock projects in cold regions [1,2]. Since the implementation of the national strategy of “One Belt, One Road”, many infrastructure projects such as highways, railroads, and open-pit mines [3] have been built in western China. However, the fact that western China belongs to a seasonal cold region with large temperature fluctuations in winter makes the outcropping rocks prone to F-T damage, so there are difficulties in maintaining rock projects in this region [4]. On the other hand, F-T damage changes the rock fracture process, which in turn affects the durability of the rock [5]. Therefore, exploring the effect of F-T damage on rock mechanical behavior and fracture processes has potential applications for engineering maintenance and safety assessment in cold regions.

Extensive research efforts have been devoted to studying the changes in the physical and mechanical properties of rocks that are exposed to F-T action in cold regions [6–9]. Huang et al. [10] carried out a series of uniaxial tests on the rock that was subjected to F-T action and found that the uniaxial compressive strength and cohesion decreased significantly. They concluded that the F-T damage was irreversible due to plastic freeze-swell deformation, which occurs below 0 °C. Lan et al. [11] investigated the effect of F-T cycles on the pore structure of red sandstone using high-pressure mercury injection tests and

concluded that macropores in the samples are more sensitive to freeze-thaw action and may affect the fracture mode of the samples. In addition, based on the test results, Xu et al. [12] found that the dynamic strength and modulus of the sandstone decreased exponentially due to the F-T action. Li et al. [13] studied the influence of pore structure evolution on the dynamic mechanical behavior of rocks using nuclear magnetic resonance and found that the evolution of pore structure leads to a decrease in the mechanical properties of rocks. The above studies have shown that the F-T effect influences the microstructure of rock, thus changing its mechanical response. In fact, rock failure is the result of the initiation and development of cracks under load until macroscopic cracks appear [14,15]. Therefore, it is important to study the effects of F-T action on the stress threshold for the development of cracks in rock. However, these studies have focused more on the changes in the macroscopic mechanical properties of rock under F-T action than on the fracture behavior, and particularly few studies have focused on rocks in the Xinjiang region.

Indeed, the application of acoustic emission technique (AE) is a reliable method to study the fracture behavior of rocks under load in the laboratory. In short, AE signals are the manifestation of microstructural behavior within the material and its intrinsic features, because intense AE behavior can reflect the fracture processes of rocks, including crushing of grains, the breakdown of pore structure, and the formation of micro-cracks [16]. Thus, several studies have explored the correlation between the F-T action and the AE signals of rocks. Su et al. [17,18] studied the effects of cyclic F-T action on the mechanical and AE behavior of granite, and reported that F-T affected the frequency-domain characteristics of the AE signals and the signals in the sample became gradually active with the increase of F-T cycles. Yang et al. [19] investigated the mechanical properties and failure processes of sandstone during thawing using the AE method and developed a damage model for frozen sandstone. Jiang et al. [20] pointed out that the critical exponent of AE probability density initially increased for each F-T cycle and then decreased with increasing cycle number by studying the damaged mechanical properties of rocks. The results of these studies have contributed to a better understanding of the effect of F-T action on AE characteristics. However, studies of crack development information that is contained in AE signals during loading are not well developed.

Considering the relative importance of F-T damage on rock materials in cold regions, this work attempts to explore the acoustic, mechanical, and physical changes that are induced by F-T action on Urumqi sandstone. First, fresh sandstone was obtained from an open-pit mine slope and then processed into standard samples. Different amounts of F-T cycles were applied to the samples. Then uniaxial compressive tests were performed and the AE signals were recorded. Finally, the effect of F-T damage on the failure attributes of the Urumqi sandstone was investigated by AE signals in the loading process.

2. Material and Methods

2.1. Material Characterization

In this study, sandstone samples that were collected from a rock slope in Urumqi in western China (Figure 1) were used to investigate the mineralogy and petrology of the rock by X-ray diffraction (Figure 2). The results showed that the rock is fine- to medium-grained with a sandy structure mainly consisting of quartz (43.8%), albite (28.5%), fraipontite (19.6%), nacrite (5.2%), and a small amount of kaolinite. The sandstone in the Urumqi region is characterized by a short formation time, weak cementation, and low strength, and has very distinct regional features [12].

To characterize the composition, distribution, size, and detrital properties of the different mineral grains of the sandstone, fabric analyses were also performed in polarized light on standard thin sections (Figure 3). The studied sandstone is mainly composed of detrital quartz grains followed by albite, with grain sizes mainly in the range of 0.05–0.25 mm. The sandstone is mainly supported by grains, and the contact between the grains is mainly planar and to a lesser extent concave-convex. The cement between the grains is dominated by kaolinite and clay, suggesting a weak cementing ability. In addition, the particle size of

the samples decreased significantly after freezing, indicating that the sandstone structure is more sensitive to F-T action. Therefore, it is reasonable to investigate the F-T action of sandstones in the Urumqi region.

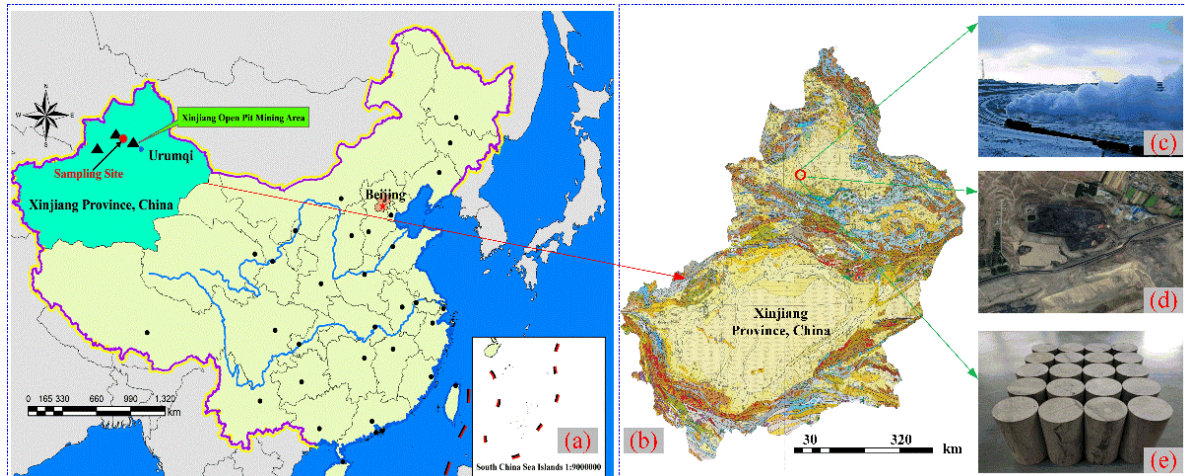


Figure 1. Location of the Xinjiang province from where the sandstone samples were obtained: (a) Location in China; (b) Detailed map of Xinjiang Province, China; (c) Actual view; (d) Satellite map of sampling point; (e) Samples. Red circle: rough location of the tested sandstone.

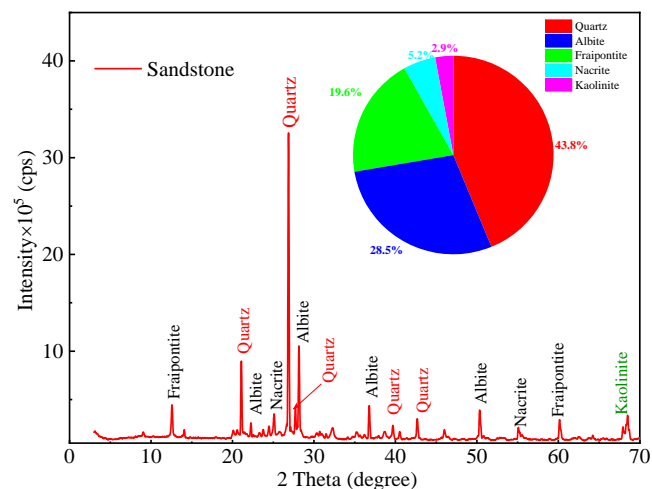


Figure 2. X-ray diffraction results for the tested sandstone.

2.2. Sample Preparation

The sandstone block that was used in this study was fresh, un-weathered, and without obvious fractures. All the tested samples were cored from the same sandstone block and then processed into cylinders with a nominal diameter of 50 ± 0.5 mm and a height of 100 ± 1 mm. According to the ISRM recommendations, the samples were ground with a tolerance of 0.02 mm for flatness at both ends, and deviations from perpendicular to the axis did not exceed 0.1% rad. To minimize the uncertainty of test results, the samples were selected before the F-T test: first, the samples with visible defects were excluded; then, the samples with similar P-wave velocities (3229 ± 50 m/s) were used by ultrasonic P-wave velocity (UPV) tests; finally, a total of 24 sandstone samples were selected and randomly divided into eight subgroups, with three samples in each subgroup. The subgroups F0, F1, F2, F3, F4, F5, and F6 represented sandstone samples with 0, 5, 10, 15, 20, 25, and 30 F-T cycles, respectively. Subgroup F7 was used to study the effect of F-T action on porosity, P-wave velocity, and the dry density of the samples.

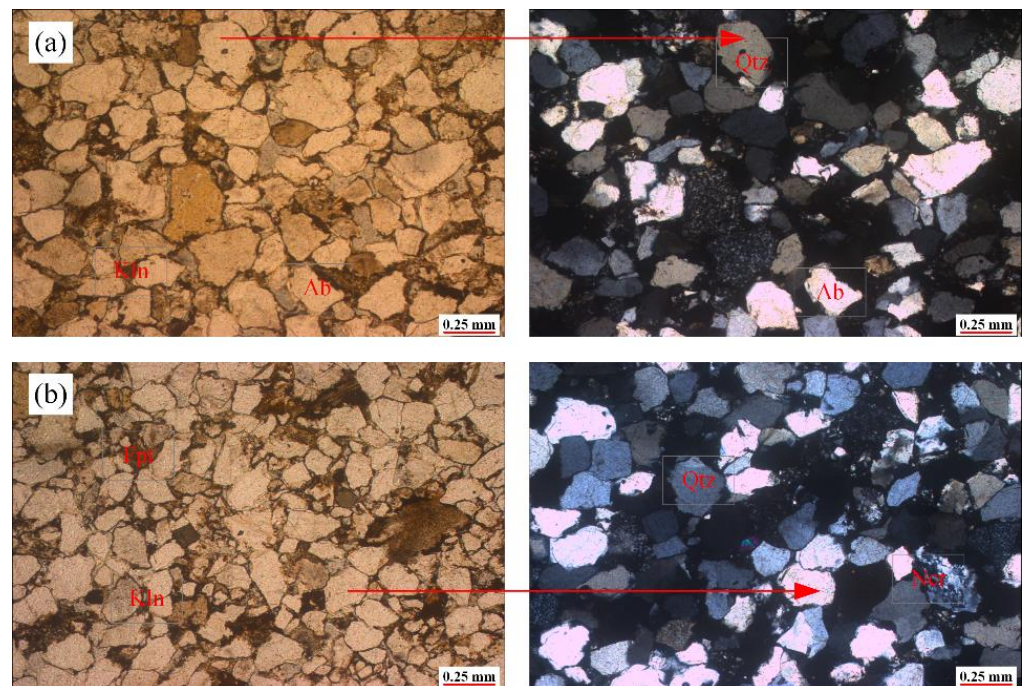


Figure 3. Thin section photomicrographs. (a) 0 F-T cycle; (b) 15 F-T cycles.

Before the F-T testing, all the samples were left to dry in an oven (110 °C) until the mass remained constant and then cooled to room temperature in a dry environment (Figure 4), while the dry mass, P-wave velocity, and volume of the sample were measured. Then, all the samples were kept in distilled water and saturated by the vacuum equipment with the fixed vacuum pressure of 100 kPa and the saturation time of 12 h [21]. Next, the samples were submerged completely in distilled water under vacuum conditions (total 24 h). Finally, the initial physical properties were obtained. The average values are listed in Table 1.

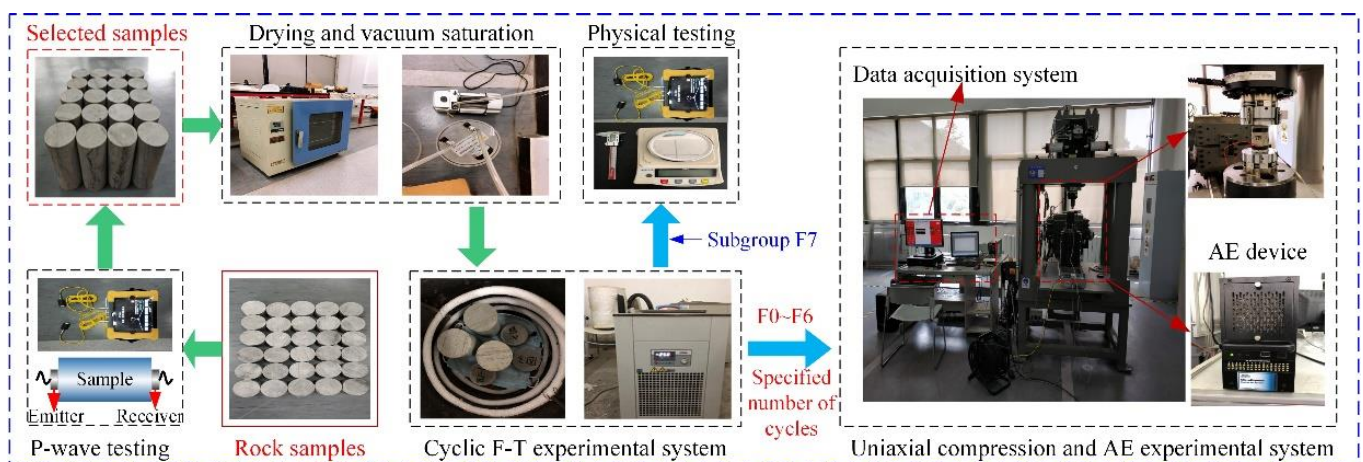


Figure 4. Experimental procedure and equipment.

Table 1. The physical parameters of the selected samples.

Parameters	V_p (m/s)	ρ_d /(g·cm ⁻³)	ρ_{sat} /(g·cm ⁻³)	ω (%)	η (%)
Range	3193~3257	2.412~2.415	2.521~2.526	4.48~4.62	4.32~4.51
Average	3229	2.414	2.523	4.56	4.37
SD	33.005	0.00125	0.00235	0.135	0.122

Notes: V_p , P-wave velocity; ρ_d , dry density; ρ_{sat} , saturation density; ω , water absorption; η , effective porosity; SD refers to the standard deviation.

2.3. Experimental Methods

2.3.1. Freeze-Thaw Cycle Tests

To investigate the influence of F-T damage on the physical and mechanical properties of the sandstone, the F-T tests were conducted on an F-T experimental system, as shown in Figure 4. Accounting for temperature fluctuations of the open-pit mine, the saturated samples were placed in the test equipment at $-20\text{ }^{\circ}\text{C}$ for 12 h and then in pure water at $20\text{ }^{\circ}\text{C}$ for 8 h to thaw, and the process was considered as one F-T cycle [22]. Each F-T cycle required 20 h to be completed. The F-T test was performed for 30 cycles on the selected samples, and their physical and mechanical properties were investigated after every 5 cycles.

2.3.2. Physical and Mechanical Tests

The compressive tests were done in a rock mechanical test system (MTS816) in the State Key Laboratory for Geomechanics & Deep Underground Engineering (Figure 4). During the test, a pair of strain gages was attached to the surface of the sample using epoxy to measure the stress-strain variations in real-time. The effective porosity of the sample with different F-T cycles was calculated by Equation (1). In addition, the P-wave velocity and dry density of the sample were determined by the tests (Figure 4).

$$n = \frac{m_s - m_d}{m_d} \times 100\% \quad (1)$$

where n is the effective porosity of the rock sample, %; m_s is the saturated mass of rock, g; and m_d is the dry mass of rock sample, g.

2.3.3. Acoustic Emission Tests

An AE measurement equipment (developed by Physical Acoustics Corporation, West Windsor Township, NJ, USA) converts energy release from the rocks into an electrical signal. This technique was used for recording the corresponding stresses at cracks closure, cracks germination, and cracks widening of the sample. In this study, both sides of each sample were attached to Nano30 sensors with Vaseline as a coupling agent and gently secured with black tape (Figure 4). The AE signals with high integrity and good matching with stress-time curves were selected for data processing. Moreover, 40 dB was selected as the monitoring threshold to avoid interference of the environment and electromagnetic noise.

3. Results and Discussion

To assess the influences of the F-T cycles on the physical and mechanical properties of the tested sandstone, a loss rate R_i was employed and used for all the physical or mechanical parameters, including porosity, P-wave velocity, dry density, and peak strength. The Equation (2) for calculating R_i is as follows:

$$R_i = \left(1 - \frac{x_N}{x_0}\right) \times 100\% \quad (2)$$

where i is the physical or mechanical property corresponding to the porosity ($i = p$), P-wave velocity ($i = v$), dry density ($i = d$), and peak strength ($i = c$); N represents the number of F-T cycles; x_N is the physical or mechanical property after N times of F-T cycles; and x_0 represents the property of samples that were not subjected to F-T action. Here it is important to note that a negative R_i means that the parameter increases with the number of F-T cycles.

3.1. Effect on the Physical Characteristics

In these tests, the porosity, P-wave velocity, dry density, and SEM images were used to assess the physical changes in the tested samples. For the samples that were subjected to 30 F-T cycles, a few cracks appeared on the surface with a small number of mineral particles

spalling (Figure 5a). Besides, the failure modes of the samples varied after different F-T cycles, showing from a shear failure to the typical tensile-shear failure (Figure 5b). As the number of F-T cycles increased, the F-T damage promoted the formation of loose structures within the sample, leading to a reduction in the internal friction angle [17]. Therefore, the angle between the failure surface and the maximum principal stress (axial direction) gradually increased, and the sample gradually changed from shear to tensile-shear failure. Furthermore, the F-T action leads to the formation of microcracks in the rock, so that the number of macroscopic cracks increases with the F-T action under load.

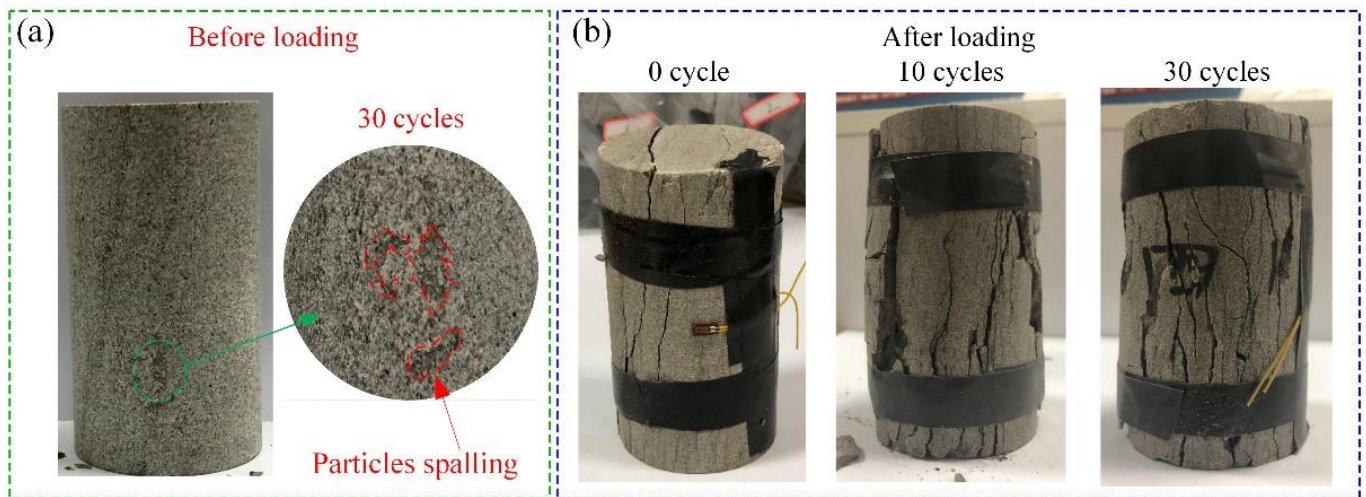


Figure 5. Failure patterns of the tested sandstone that was subjected to different numbers of F-T cycles. (a) Before loading; (b) After loading.

3.1.1. Effect on the Porosity

The average porosity of the tested sample versus the number of F-T cycle is shown in Figure 6. From that, the porosity presented an increasing trend with an increase in the F-T cycle number. After 30 F-T cycles, the average porosity of the tested sandstone increased by 13.7%, suggesting an increase in the volume of pores within the sandstone sample. This means that irreversible damages occurred in the samples during the process of freezing or thawing [23], and these damages within the rocks embodied the work that was done by the frost heave force. Further, the change of stress path within the samples during loading due to the existence of defect spaces explained the different failure modes with the number of F-T cycles as presented in Figure 5. Besides, during cyclic F-T tests, some mineral components on the pore wall of the sample dissolved in pore water, leading to damage and deterioration of the weak pore wall [13]. Thus, crystallization pressures that were generated by the ice and exerted on the pore walls caused the generation of more pore space, which in turn leads to the decrease of the overall (tensile) strength of the rock.

3.1.2. Effect on the Micro-Morphology

The variations in the micro-morphology of the sandstone samples under different F-T action were studied using the scanning electron microscope (SEM) images (Figure 7). The results from the SEM images revealed that the F-T action had an important effect on the surface morphology of the tested sandstone with the induction of more defects suffered under increasing F-T cycles. The density of the micro-cracks under F-T action expanded to a considerable extent. In particular, the transition from intergranular to transgranular cracks in the micro-morphology indicated that stronger F-T action can not only affect the cement strength but also decrease the strength of mineral particles. The damage of cement and mineral particles provided favorable conditions for crack development and was embodied in widening the F-T crack aperture. Besides, the variations of micro-morphology in images also explained the increase of porosity in Figure 6.

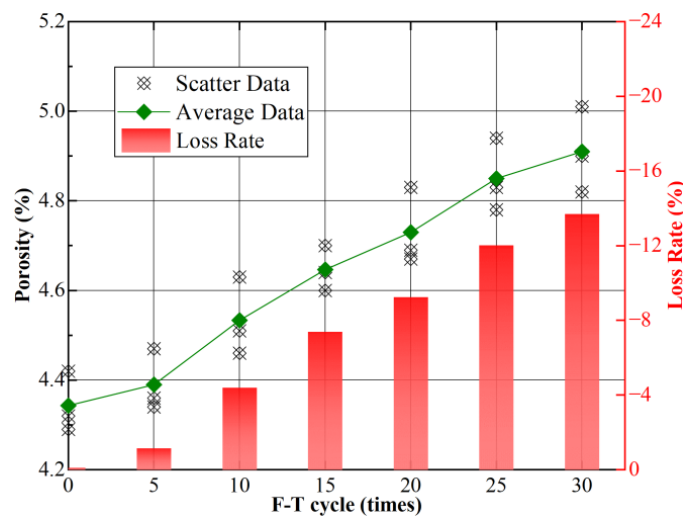


Figure 6. The average porosity and loss rate with cycles in tested sandstone.

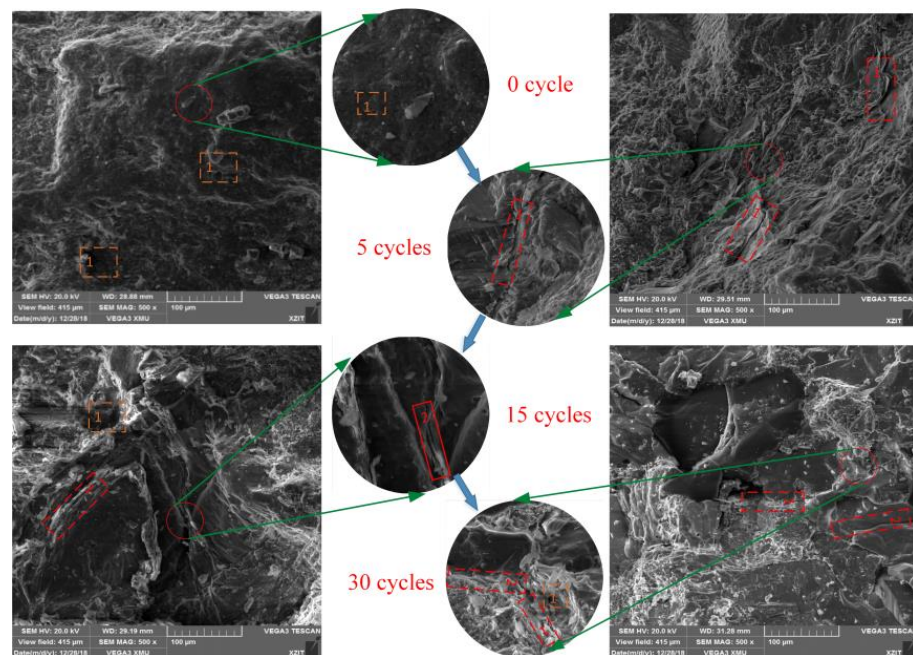


Figure 7. SEM micrographs of sandstone samples under F-T actions. Orange frame 1: pore; Red frame 1: intergranular fracture; Red frame 2: transgranular fracture.

3.1.3. Effect on P-Wave Velocity

The physical parameter P-wave velocity was sensitive to the micro-morphology in the medium, so it can be used as an appropriate indicator to examine the damage on the microscopic scale [24]. In this study, the P-wave velocity was used to understand the degree of cracking with F-T action. Figure 8 showed the average P-wave velocity with the different number of F-T cycles and reflected that the F-T action significantly affected the P-wave velocity of the samples. From that, the P-wave velocity showed a decreasing trend under F-T action, with the average P-wave velocity decreasing by 5.8% after 30 F-T cycles. With increased crack density, however, the P-waves reflected, refracted, diffracted, or scattered through cracks in the medium, and the corresponding P-wave velocity slowed down [25]. Therefore, the variation in Figure 8 signified that plenty of micro-cracks have formed inside the tested samples. In addition, the decrease in P-wave velocity also indicated the reduction in the microstructural density of the tested samples that were subjected to F-T action.

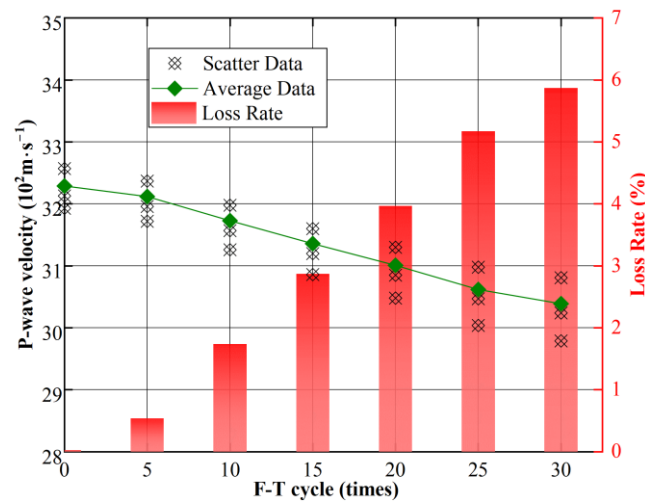


Figure 8. The average P-wave velocity and loss rate with cycles in the tested sandstone.

3.1.4. Effect on Dry Density

The dry density of the tested sandstone under different F-T cycles had a decreasing trend in Figure 9. The curve showed that the change range of the first two data was significantly larger than that of the later data, showing a fast change, followed by a slow trend. This phenomenon suggested that F-T damage of the samples that was caused by fewer F-T cycles occurs mainly on the surface of the samples, because some mineral particles on the surface are easily detached in the early stage of F-T cycles, as shown in Figure 5a. The change curve also indicated the development process of F-T damage from the surface to the inside [17].

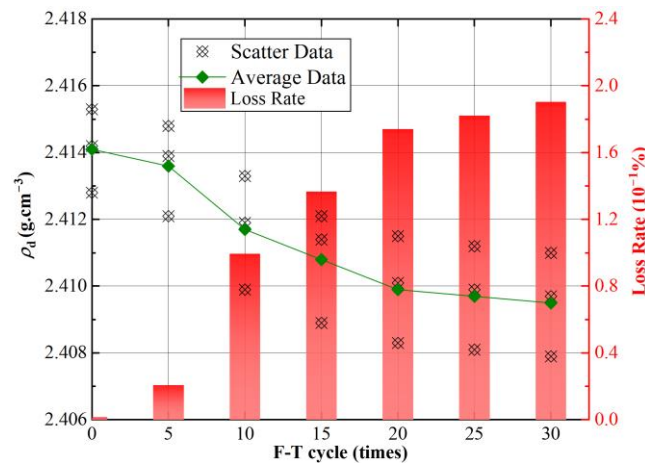


Figure 9. The average dry density and loss rate with cycles in the tested sandstone.

In general, the F-T damage of rocks is mainly affected by the following factors: lithology, moisture content, number of F-T cycles, ionic solution, temperature range, and stress state [26,27]. When the samples were completely frozen, the frost heave force occurred in the pore sides for the increase of ice volume (about 9%), promoting further development and expansion of initial defects to form new micro-cracks [5]. On the other hand, when the temperature decreased, inconsistent deformation appeared among different mineral particles due to their different thermal expansion properties [9]. At the same time, the expansion of ice volume aggravated this deformation, resulting in huge local crystallization pressures (i.e., frost heave force) among the mineral particles or micro-cracks. The pressures acted on the microscopic scale of mineral particles or micropores of the rocks. Therefore, the presence of pore water had a profound effect on the rock damage under the F-T cycle conditions [28]. If there is no water in the pores or micro-cracks, there is no so-called F-T

damage, i.e., dry rocks are hardly affected by F-T cycles [29]. When the temperature rose, the ice in the pores or micro-cracks melted, accompanied the release of frozen stress and the migration of water, thus accelerating the damage [30]. After repeated F-T cycle tests, therefore, numerous defects inside the samples caused the changes in physical properties that were mentioned above.

3.2. Effect on the Mechanical Behavior

In this part, the results are combined with the F-T numbers to explore the changes in the mechanical behavior with the F-T damage. Moreover, the peak stress and elastic modulus of the tested sandstone samples are also discussed.

3.2.1. Stress-Strain Behavior

The stress-strain behaviors of the samples that were subjected to F-T action are presented in Figure 10, indicating that the F-T action significantly affects the pre-peak stress-strain relations of the sandstone samples. All the curves showed a non-linear behavior in the initial compressive stage and exhibited a consistent variation due to the increasing F-T treatments. The stress-strain curves became gradually more non-linear with an increasing number of applied F-T cycles, indicating that the number of pores or cracks in the samples increased with F-T action. On the other hand, the crack closure strain increased with more F-T cycles, which can be used to evaluate the density of cracks and further identify the amount of cracks damage in the rocks [31]. Moreover, the non-linear stage near the peak stress showed a clear increasing trend with the F-T action, signifying that part of the energy was consumed after the elastic stage in the loading process; these energies were closely related to the porosity, damage degree, mineral particles, and cement strength of the sample. Li et al. [32] considered that the crack propagation and frictional increase among mineral particles in samples were primarily responsible for the energy consumption near the peak stress. For the samples that were subjected to F-T action, the microstructures inside the rock changed from relatively dense to loose (Figure 7). Meanwhile, the peak strain corresponding to peak stress tends to increase with F-T action, signifying a larger deformation in rocks with more F-T cycles (Figure 10). These variations that were induced by F-T action facilitated the development of cracks, so the variations of non-linear behavior near peak stress reflected the significant effect of F-T action on the microstructure in the tested sandstone. Besides, the slope in the linear stage of the stress-strain curves decreased with the increase of F-T action number, indicating a reduction in the elastic modulus.

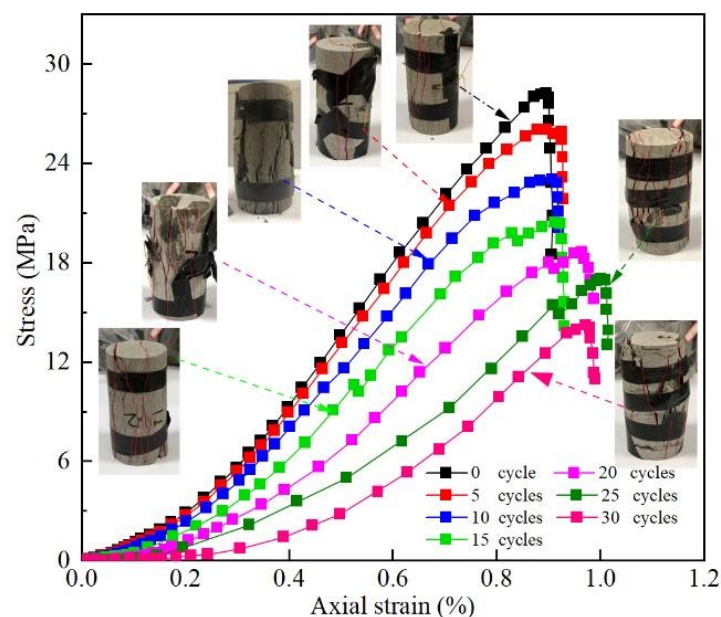


Figure 10. Stress-strain curves of the tested samples that were subjected to different F-T cycles.

3.2.2. Mechanical Behavior after F-T Action

There have been many studies about the decline in the mechanical behavior with F-T damage in different rocks [33,34]. This decreasing trend can be attributed to the development of cracks in the rocks that is caused by the F-T action. In this research, the peak stress for the tested sandstone sample also decreased with the increasing F-T action [35]. In Figure 11, there is a negative correlation between the peak stress and the F-T cycle number of the tested samples, with the sample under 5 F-T cycles showing a minor mechanical deterioration (about 6.9%), and the sample suffered 30 F-T cycles having a larger loss (about 49%) in the peak stress. Zhang and Yang [36] argued that the combined effect of F-T action and loading aggravated the total damage of the rock with obvious non-linear characteristics, whereas its coupling effect weakened the total damage. Moreover, the variation in the stress path that was caused by the F-T cracks was vitally important on the peak strength decrease of the tested samples at high F-T damage.

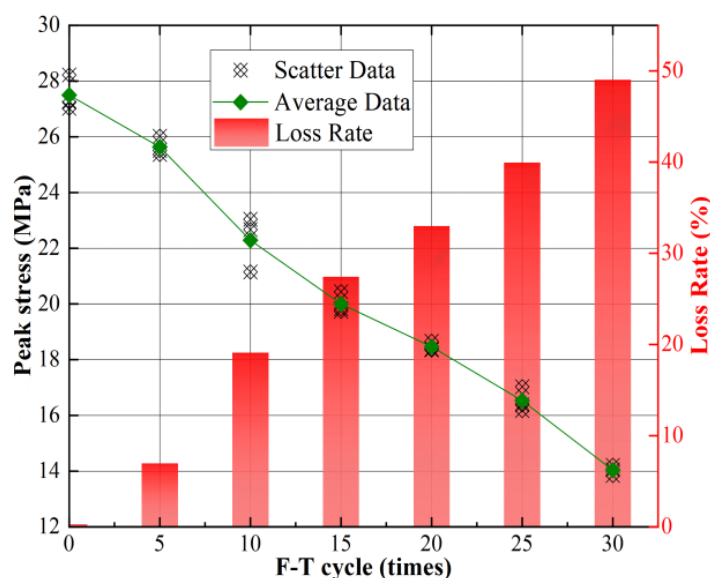


Figure 11. Change in the peak stress and loss rate with F-T action in the tested sandstone.

As shown in Figure 12, a schematic diagram of the freezing sequence of the ‘main-side branch’ was developed based on the size of the pore structure. The F-T damage in sandstone is the result of a combination of capillary, crystal pressure, hydrostatic, and volumetric expansion mechanisms [13]. When the temperature drops below 0 °C, the main pores initially freeze as ice by heterogeneous nucleation due to their greater curvature [27]. At this time, the ice in the pores drives the unfrozen water to form seepage damage on the pore wall, which is known as the hydrostatic pressure mechanism. The volumetric expansion mechanism, on the other hand, is the damage that is caused by the volumetric expansion of the ice [9]. Since the chemical potential of the water in the small pores is higher than that of the pore ice in the main pores, the supercooled water from the small pores migrates through the pellicular water into the main pores, promoting further development of the structural damage in the pores [27]. The capillary mechanism plays an important role in this process. In addition, when the pore ice develops into secondary pores, the growth of the pore ice causes a hydraulic fracturing effect at the pore tips when the secondary pores are closed [5]. As the F-T effect increases, the damage to the pore structure in the sandstone increases. Thus, as mentioned above, there are significant differences in the physical and mechanical behavior of sandstone under loading.

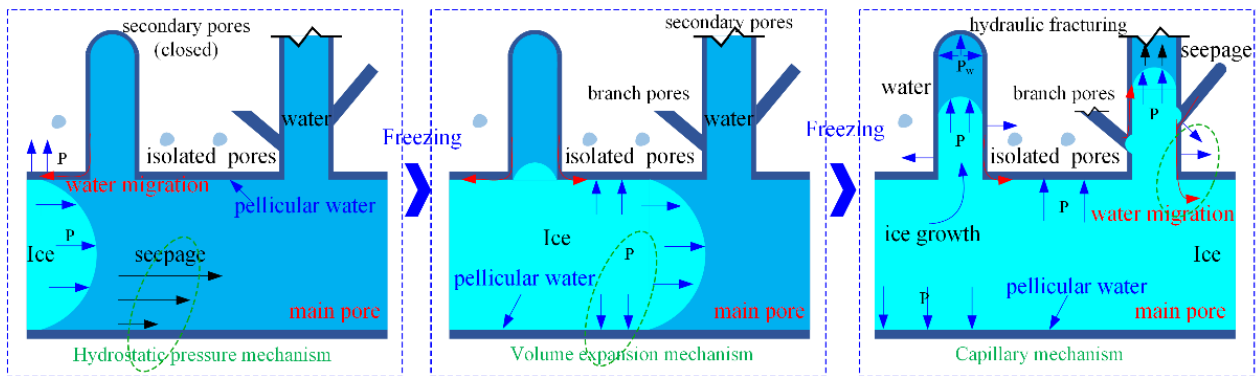


Figure 12. F-T damage mechanism.

Besides, the elastic modulus showed a negative correlation with the increasing number of F-T cycles (Figure 13a). This indicates a considerable reduction in the deformation resistance of the studied samples that was induced by the F-T process. Additionally, the F-T damage (D_N) was estimated using the empirical Equation [22]. The empirical Equation is as follows:

$$D_N = 1 - \frac{E(N)}{E(0)} \tag{3}$$

where D_N is the damage under the F-T action; $E(0)$ is the elastic modulus of the fresh rock; and $E(N)$ is the elastic modulus of the rocks that are subjected to N F-T cycles. The F-T damage for the tested samples exhibited an increase with increasing F-T cycle number (Figure 13b), and a prediction model was developed for damage changes.

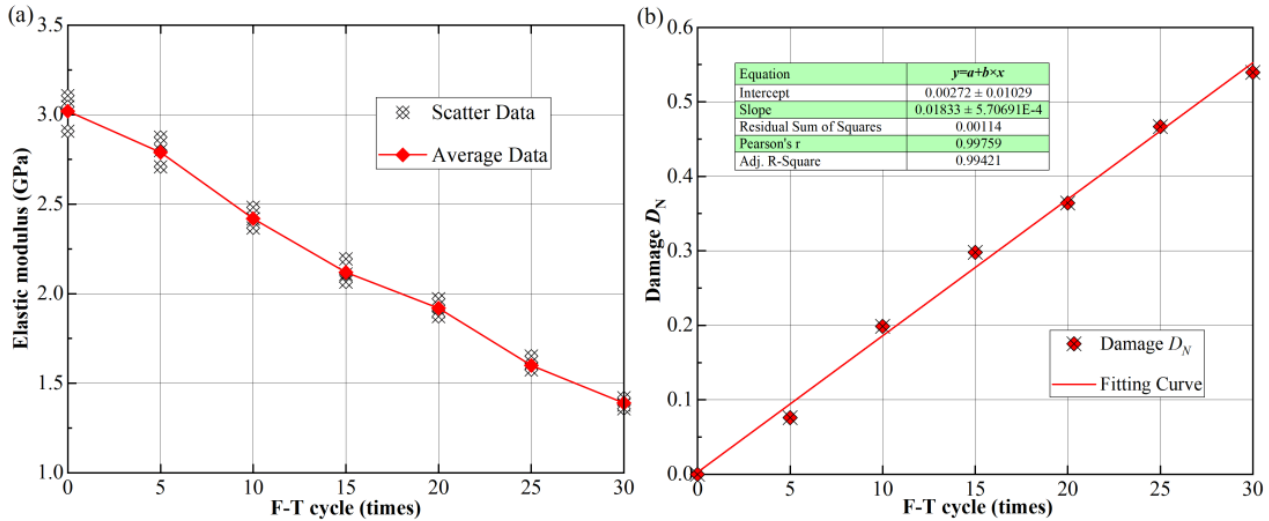


Figure 13. Variation of the elastic modulus (a) and damage (b) with F-T cycles.

3.3. Physical and Mechanical Prediction Model

To describe the relationship between the F-T action and the rock properties, Mutlutürk et al. [37] developed a decay model to characterize the decay rate of different sandstones, incorporating the decay constant and half-life, as shown in Equation (4):

$$- (dI/dN) = \lambda I \tag{4}$$

where the minus sign indicates a decrease in the rock integrity; I denotes the rock integrity; N denotes the number of F-T cycles; and λ denotes the decay constant.

If the integrity of the sample prior to applying the F-T cycles is I_0 , it is I_N after N F-T cycles. By integrating Equation (4), the decay model can be expressed in an exponential formula, Equation (5):

$$I_N = I_0 e^{-\lambda N} \quad (5)$$

In addition, another useful parameter, half-life ($H_{1/2}$), is defined as the number of cycles that are necessary to halve a physical or mechanical property and is introduced to measure the long-term durability of the rock. This durability parameter (half-life) is inversely proportional to the decay constant and can be calculated by using $I_0/2$ to replace the I_N in Equation (6) as follows:

$$H_{1/2} = \ln 2 / \lambda \approx 0.693 / \lambda \quad (6)$$

Given that the integrity of rock involves physical and mechanical properties, the degradation characteristics of properties such as the P-wave velocity, density, strength, and deformation modulus of rocks under F-T action also fit Equation (5). The degradation characteristics are shown in Table 2. The half-life of the elastic modulus is only 27 cycles compared to other parameters such as density and strength, indicating that the deformation resistance of this sandstone to F-T damage is more pronounced. At the same time, the decay factor of the elastic modulus is 0.0254, which is much higher than the decay factor of P-wave velocity and density. Therefore, rock deformation in open pit mining in this area must be carefully monitored.

Table 2. Relationships among the physical and mechanical parameters with F-T cycle.

Parameter	Fitted Curves	Decay Factor	Half-Life ($H_{1/2}$)	R^2
P-wave v	$v = 3237.7 \cdot \exp(-0.00214 \cdot N)$	0.00214	324	0.987
Density ρ	$\rho = 2.414 \cdot \exp(-6.97 \times 10^{-4} \cdot N)$	0.000697	994	0.912
Strength σ	$\sigma = 27.924 \cdot \exp(-0.0217 \cdot N)$	0.0217	32	0.991
Modulus E	$E = 3.092 \cdot \exp(-0.0254 \cdot N)$	0.0254	27	0.989

As mentioned earlier, the deformation, failure behavior, and mechanical properties of the tested sandstone under loading were all affected by F-T action. These variations can be attributed to changes in the stress threshold for crack initiation, propagation, and failure during loading [38]. To deeply understand this process, the changes in the AE parameters were combined with stress to explore further the variations in crack germination, propagation, and failure degree that was caused by the freezing or thawing damage in the loading process for the tested sandstone.

3.4. Effects on the AE and Failure Behavior

Since the F-T damage complicates the fracture processes in the tested samples, understanding the fracture behavior under loading is crucial. The acoustic signal can offer abundant information concerning the fracture processes and the associated stages of deformation in rocks [38]. The dynamic monitoring of the rock deformation and fractured space evolution in the loading process using AE data has become a useful method for damage evaluation. As shown in Figure 14, a possible relationship between AE activity and stress-strain behavior during loading deformation was observed by Boyce et al. [39]. Therefore, this study employed AE technology to understand the variations in stress thresholds for fracture processes (cracks germination propagation and damage) that were caused by F-T action. Thus, the changes in AE signals were carefully studied and evaluated with Figure 13 in mind, and these results were then related to the damage that was done to the samples by the F-T cycles.

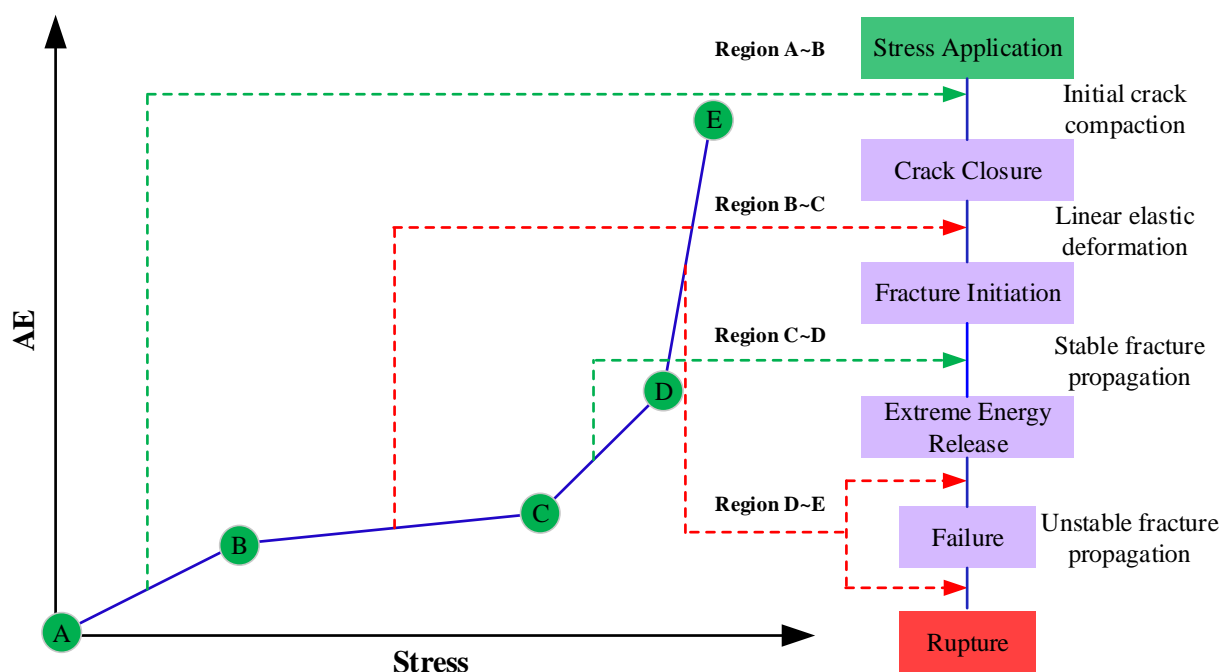


Figure 14. The relationship between the AE signal and stress with rock deformation (after [39]).

3.4.1. Acoustic Behavior

The AE and cumulative AE responses over the time of samples during the loading process were drawn in Figure 15a–d. The variation in AE counts under different F-T cycles can be divided into three regimes, including the initial period, quiet period, and active period. During loading, the AE counts became more active in the samples that experienced more F-T cycles, which was reflected in the increasing cumulative AE counts. In the initial loading period, the AE counts were a result of friction among the particles for the micro-cracks closure within the rock. In Figure 15, the AE counts showed a significant increase with the F-T cycles in the initial period, suggesting that F-T action promoted the development of microscopic defects (tensile micro-cracks) in the sample, thereby affecting the variation of AE counts [17]. After the initial crack closure, the AE activity entered the quiet period in which the elastic energy is being accumulated in the sample. This continues until the required energy or stress for crack growth is reached. However, as the number of F-T cycles increased, the density of AE counts in the quiet period also increased, with more abrupt points appearing before the failure of the sample (Figure 15d). In this process, a part of the energy was released by a stress waveform, resulting in a sharp increase in AE counts. This interesting phenomenon indicated that tested samples were about to enter the stage of unstable crack development and gradually reach the peak stress point to produce failure. Moreover, it can be observed that the duration of the active period was influenced by the F-T effects and showed an increasing trend. Therefore, the changes in AE behavior due to the F-T action need to be taken into account in the monitoring and warning of rock projects to avoid misjudgments in the cold regions.

3.4.2. Variation in Acoustic Properties and Damage Stress

The acoustic profiles that were obtained from uniaxial compressive tests are shown in Figure 16. The deduction of F-T damage based on acoustic signals was divided into four stages following Figure 14 [40], including (I) crack closure stage where some acoustic signals were recorded; (II) new cracks began to appear, showing an increase in acoustic signals; (III) interaction among cracks began to intensify, resulting in micro-cracks propagation and coalescence with lots of acoustic signals; and (IV) the appearance of macro-cracks led to unstable fracture propagation resulting in final failure. Figure 16 presents an obvious demarcation and a different variation in the AE-stress relationship of the sample with a

different amounts of FT cycles applied, indicating that the F-T damage has a vital effect on the fracture process of the tested samples, including micro-crack initiation, their coalescence, propagation, and eventually macro-cracks formation. Consequently, the tested samples exhibited different deformation behavior under loading with the variation of the F-T damage. Here, it is necessary to point out that visible damage refers to the propagation of the macro-cracks. Besides, the crack germination stage (II) of the sample decreased with the increasing F-T action, while the macro-cracks damage zone (IV) widened with the increasing F-T cycles. As the compression progresses, the AE rate that was produced by the test samples decreased significantly due to the coalescence of micro-cracks in stage II [41]. When the samples entered the failure phase, the deformation changed from micro-cracks coalescence to micro-cracks propagation, forming macro-cracks damage zones, while the AE rate showed a dramatic increase. The extent of F-T damage dramatically affected the macro-cracks generation and subsequent propagation. Therefore, these results proved that the F-T damage largely controls the AE behavior of the tested samples under uniaxial compressive loads.

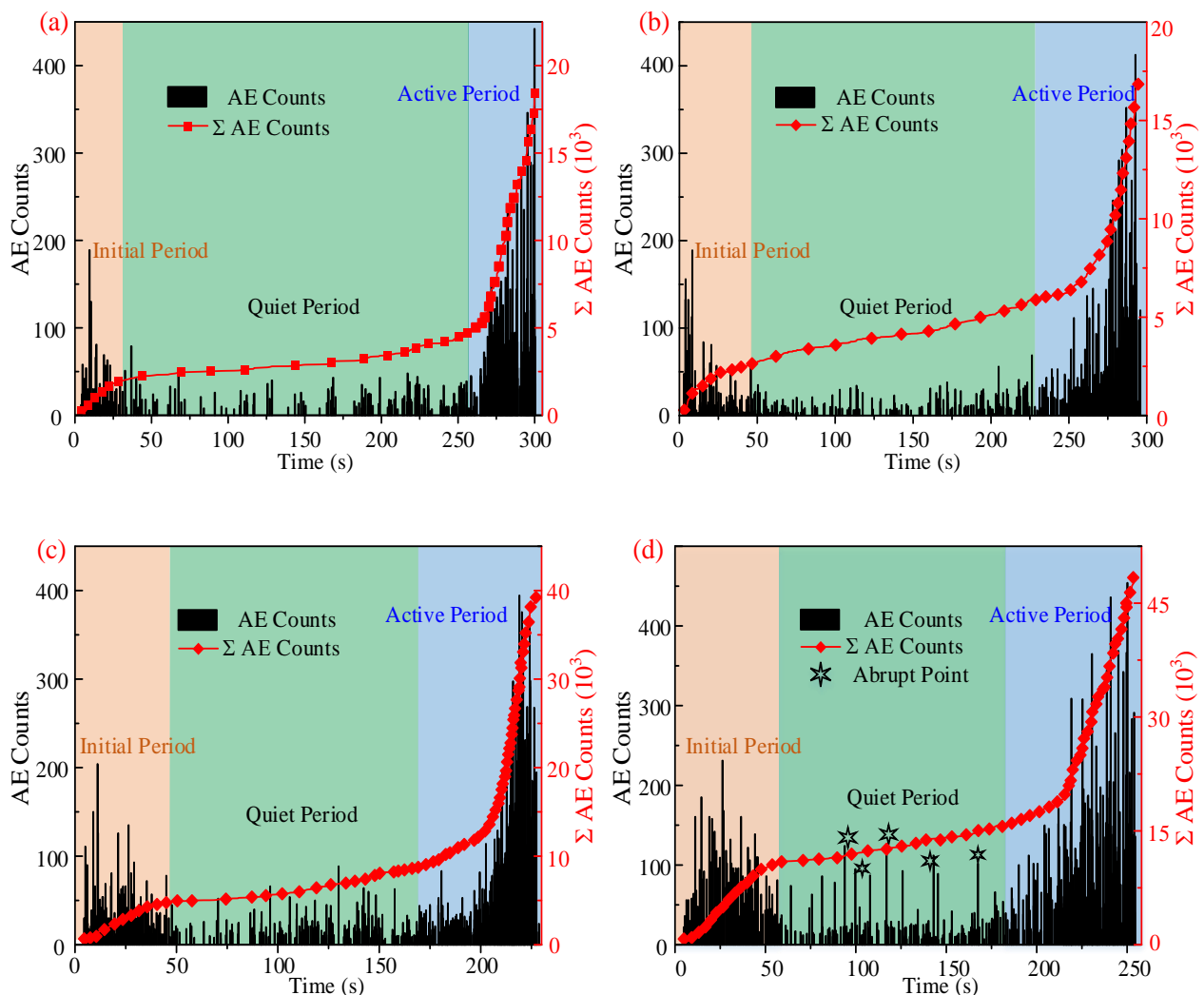


Figure 15. Relationship between the AE counts, cumulative AE counts, and the time of samples with different numbers of F-T cycles under uniaxial compression condition: (a–d) represent the tested samples that were subjected to 0, 5, 15, and 30 F-T cycles, respectively.

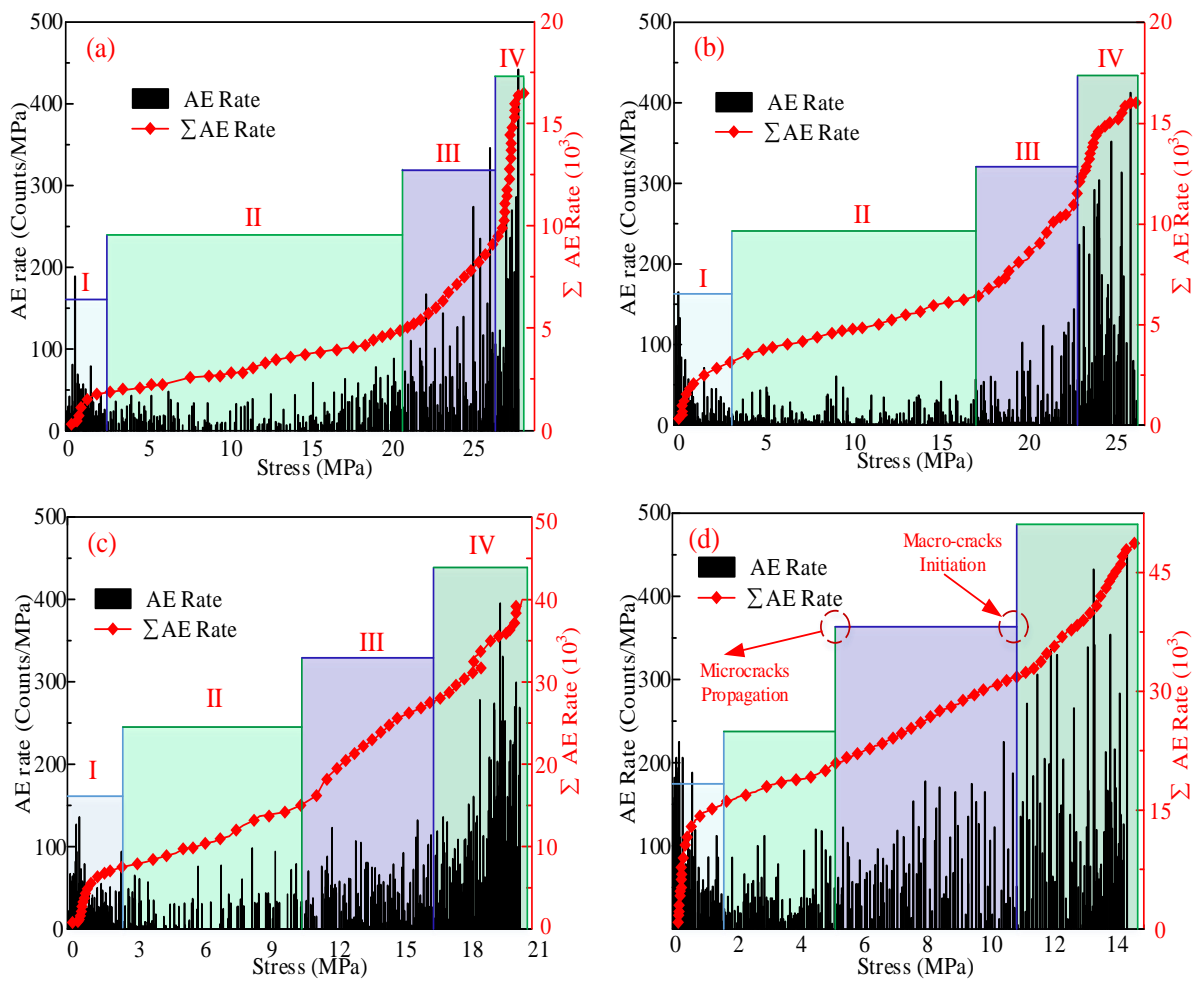


Figure 16. The relationship between the AE behavior and the stress of samples with different F-T cycles under uniaxial compression conditions: (a–d) represent the samples that were subjected to 0, 5, 15, and 30 F-T cycles, respectively.

Furthermore, the crack propagation of the sample under loading was varied with F-T cycles. The tested samples without F-T damage showed an obvious elastic deformation (II) process and prolonged the initiation and coalescence of micro-cracks but limited micro-cracks propagation and macro-cracks initiation (Figure 16a). These results indicated that the samples in the fresh state require sufficient stress to provide energy for the micro-cracks propagation before the failure, i.e., it is hard for micro-cracks of untreated samples to propagate due to the stability of the sample microstructure. However, with the increase of F-T action, the elastic deformation tended to decrease (II), while the propagation phase of the micro-cracks presented an increasing trend with a high AE rate before sample failure (III stage). This was probably due to the volumetric expansion that was introduced by the phase transformation of the water and ice in the cracks or pores [1]. These processes promoted the initiation and coalescence of micro-cracks, thereby reducing the energy that was provided by stress in the elastic deformation stage. As the study of Fang et al. [22], the F-T action had a significant deterioration effect on the bonding strength of rocks. This conclusion strongly proved that the F-T damage caused a decrease of resistance to the micro-cracks growth under loading, thereby facilitating the micro-cracks to initiate and coalesce (stage II) effortlessly with less stress input, matching with Figure 16. At the same time, the deterioration of the bonding and particles in the samples promoted the micro-cracks initiation and propagation. These microstructures then produced sliding friction under loading, resulting in increased energy consumption that was manifested in the extension

of the III and IV stages. Additionally, the generation of friction between the cement and particles well explained the increasing AE rate.

The cumulative AE parameters against stress values under loading are shown in Figure 17. With increasing F-T damage, the AE signals showed a continuous transition during loading, corresponding to the different stages of crack development. The cumulative AE rates increased with increasing F-T damage, except in the pre-peak stage. This is due to the fact that F-T damage changes the brittleness of the rock and prolongs the macroscopic crack failure phase before the peak. To better understand the variations in the AE behavior of the samples as a result of F-T action, the normalized stress values were plotted against the normalized cumulative AE rate. This plot provided helpful insight into identifying the stress levels at which fracturing changes due to F-T damage. Figure 17b showed that the acoustic properties of all the samples under F-T action follow an identical pattern. This indicated that the fracture tendency shifts at 70% to 95% of the peak stress. In addition, F-T damage led to early crack development. All the tested samples exhibited drastic AE rates in the initial stage, which gradually decreased after reaching the crack extension stress. To determine the effect of F-T damage on the crack development of the sample during loading, the point of AE transition was chosen as the stress threshold for crack development according to Figure 14, as shown in Figure 18.

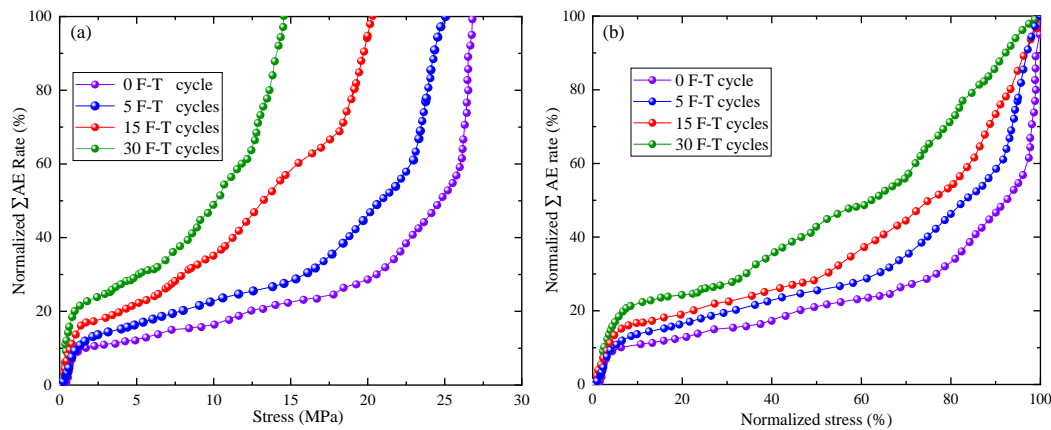


Figure 17. Changes in the acoustic behavior and stress with different F-T cycles. (a) Stress; (b) Normalized stress.

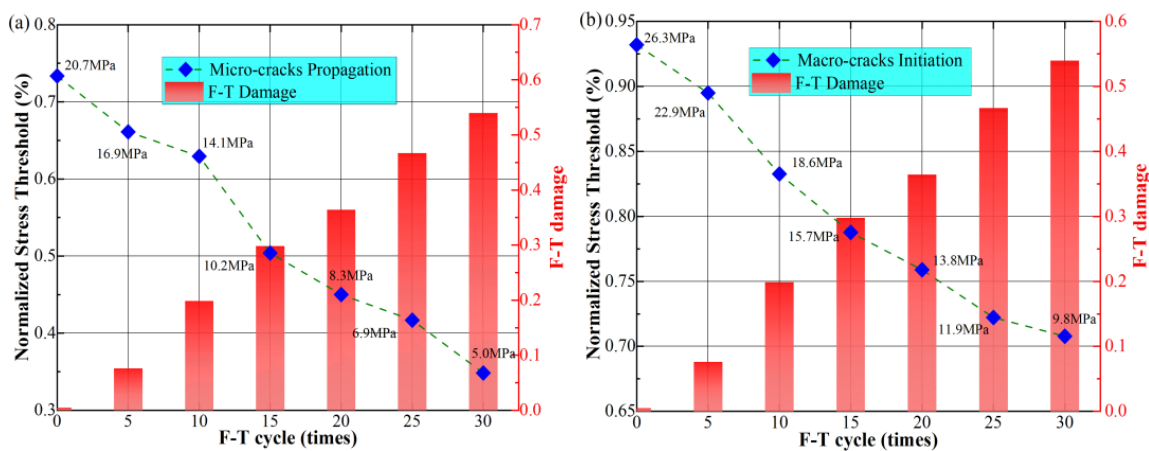


Figure 18. Acoustic behavior of the sandstone that was subjected to different F-T action. (a) Micro-cracks; (b) Macro-cracks.

As Sirdesai et al. [38] reported, the stress threshold was helpful to determine the onset, coalescence, and propagation of the micro-cracks in rocks. Therefore, this study focused on the stress threshold of the sandstone in each deformation stage by analyzing the change

of AE behavior with the F-T cycles. At the same time, the stress threshold values were normalized by the peak stress to better understand the effect of F-T damage on them. Figure 18 shows the stress threshold values corresponding to each shift point in the loading process. From that, with the increase of F-T damage, the stress threshold for micro-cracks propagation and micro-cracks initiation decreased obviously. For example, the normalized stress threshold for micro-cracks propagation decreased from 0.734 (20.73 MPa) to 0.348 (5.04 MPa) after 30 F-T cycles. Also, the normalized stress threshold for macro-cracks initiation dropped from 0.932 (26.3 MPa) to 0.708 (9.8 MPa) after 30 F-T cycles. These phenomena indicated that micro-cracks appeared in rocks even under low-stress inputs with the increase of F-T damage, resulting in reducing the load-bearing capacity and strength. The strength can be considered as the result of the particle, bonding strength, and the particle chimeric action. However, with more F-T treatment, the stress-strain curves witnessed a diminishing trend of peak stress, signifying the deterioration of the mineral particle strength and bonding among minerals. Meanwhile, this degradation of strength can be considered as a change in rock brittleness on the stress-strain curve. Li et al. [32] believed that this change indicated that the rocks absorbed more energy before failure. Thus, the macro-cracks damage zone (III) enlarged with the increase of F-T damage under the loading process in Figure 16. After 30 F-T cycles, the macro-cracks damage zones increased from 7% (IV) under fresh conditions to 29%. The sandstone sample witnessed about a 76% increase in macro-cracks damage zones. These results strongly proved that the F-T damage has a substantial impact on the fracture behavior of typical sandstone samples in Xinjiang, China.

4. Conclusions

In cold regions, the changes in the physical and mechanical properties of rocks under F-T action often lead to some rock engineering disasters. In this study, the sensitivity of physical and mechanical properties of sandstone in Urumqi to F-T action was investigated. In addition, the evolution of stress thresholds for crack initiation and development in the sandstone with F-T cycles was analyzed based on AE-stress relationships. The main conclusions are as follows:

1. In the Urumqi region, the elastic modulus of the rock is more sensitive to F-T cycles than other physical-mechanical parameters such as density and strength, which have a half-life of only 27 cycles. Therefore, special attention should be paid to the rock deformation to prevent open-pit mining disasters.
2. The acoustic behavior of the studied sandstone clearly shows the effect of F-T cycles on the AE-stress relationship. As F-T damage increases, the crystallization pressure that was induced by freezing forms cracks, making the crack closure phase more pronounced with larger cumulative AE rate values. Subsequently, with the load increases, micro-cracks begin to develop and expand, forming visible crack damage zones on the surface.
3. The stress thresholds for micro-crack development and macro-crack initiation decrease with the increasing F-T damage. After 30 F-T cycles, the stress threshold for micro-cracks propagation decreases from 20.73 MPa in the natural condition to 5.02 MPa, while that of the macro-cracks damage zone increases from 7% to 29%. The F-T damage has an important impact on the fracture behavior of typical sandstone samples from Xinjiang, China.

Author Contributions: Methodology, J.X. and H.P.; investigation, Z.S.; resources, J.X.; data curation, Z.S. and J.X.; writing—original draft preparation, J.X.; writing—review and editing, J.X. and H.P.; visualization, Z.S. and J.X.; supervision, H.P. All authors have read and agreed to the published version of the manuscript.

Funding: This research was funded by the National Natural Science Foundation of China (No. 51974296, No. 52061135111).

Data Availability Statement: Data available on request due to privacy restrictions.

Conflicts of Interest: The authors declare no conflict of interest.

References

1. Momeni, A.; Abdilor, Y.; Khanlari, G.R.; Heidari, M.; Sepahi, A.A. The effect of freeze–thaw cycles on physical and mechanical properties of granitoid hard rocks. *Bull. Eng. Geol. Environ.* **2016**, *75*, 1649–1656. [[CrossRef](#)]
2. Jiang, H.; Li, K.; Jin, J. The variation characteristics of micro-pore structures of underground rocks in cold regions subject to freezing and thawing cycles. *Arab. J. Geosci.* **2020**, *13*, 17. [[CrossRef](#)]
3. Chang, Z.; Zhang, W.; Zhao, G.; Dong, F.; Geng, X. Aging Stability Analysis of Slope Considering Cumulative Effect of Freeze–Thaw Damage—A Case Study. *Minerals* **2022**, *12*, 598. [[CrossRef](#)]
4. Lu, Y.; Li, X.; Chan, A. Damage constitutive model of single flaw sandstone under freeze-thaw and load. *Cold Reg. Sci. Technol.* **2019**, *159*, 20–28. [[CrossRef](#)]
5. Hallet, B. Why do freezing rocks break? *Science* **2006**, *314*, 1092–1093. [[CrossRef](#)]
6. Karaca, Z.; Hamdi Deliormanli, A.; Elci, H.; Pamukcu, C. Effect of freeze-thaw process on the abrasion loss value of stones. *Int. J. Rock Mech. Min. Sci.* **2010**, *47*, 1207–1211. [[CrossRef](#)]
7. Gao, F.; Xiong, X.; Zhou, K.P.; Li, J.L.; Shi, W.C. Strength deterioration model of saturated sandstone under freeze-thaw cycles. *Rock Soil Mech.* **2019**, *40*, 926–932.
8. Laskaridis, K.; Arapakou, A.; Patronis, M.; Kouseris, I. Correlations between the Physical Mechanical Properties of Greek Dimension Stones. In Proceedings of the International Conference on Raw Materials and Circular Economy, Athens, Greece, 5–9 September 2021; p. 28.
9. Khanlari, G.; Abdilor, Y. Influence of wet–dry, freeze–thaw, and heat–cool cycles on the physical and mechanical properties of Upper Red sandstones in central Iran. *Bull. Eng. Geol. Environ.* **2015**, *74*, 1287–1300. [[CrossRef](#)]
10. Huang, S.; He, Y.; Liu, X.; Xin, Z. Experimental investigation of the influence of dry-wet, freeze-thaw and water immersion treatments on the mechanical strength of the clay-bearing green sandstone. *Int. J. Rock Mech. Min. Sci.* **2021**, *138*, 104613. [[CrossRef](#)]
11. Lan, Y.; Gao, H.; Zhao, Y. Pore Structure Characteristics and Strength Variation of Red Sandstone under Freeze–Thaw Cycles. *Materials* **2022**, *15*, 3856. [[CrossRef](#)]
12. Xu, J.; Pu, H.; Sha, Z. Mechanical behavior and decay model of the sandstone in Urumqi under coupling of freeze–thaw and dynamic loading. *Bull. Eng. Geol. Environ.* **2021**, *80*, 2963–2978. [[CrossRef](#)]
13. Li, J.; Kaunda, R.B.; Zhou, K. Experimental investigations on the effects of ambient freeze-thaw cycling on dynamic properties and rock pore structure deterioration of sandstone. *Cold Reg. Sci. Technol.* **2018**, *154*, 133–141. [[CrossRef](#)]
14. Si, K.; Cui, Z.; Peng, R.; Zhao, L.; Zhao, Y. Crack Propagation Process and Seismogenic Mechanisms of Rock Due to the Influence of Freezing and Thawing. *Appl. Sci.* **2021**, *11*, 9601. [[CrossRef](#)]
15. Chen, L.; Wu, P.; Chen, Y.; Zhang, W. Experimental Study on Physical-mechanical Properties and Fracture Behaviors of Saturated Yellow Sandstone Considering Coupling Effect of Freeze-Thaw and Specimen Inclination. *Sustainability* **2020**, *12*, 1029. [[CrossRef](#)]
16. Baud, P.; Klein, E.; Wong, T.F. Compaction localization in porous sandstones: Spatial evolution of damage and acoustic emission activity. *J. Struct. Geol.* **2004**, *26*, 603–624. [[CrossRef](#)]
17. Su, Z.; Sun, J.; Xia, J.; Wu, C. Experimental research of the effect of freezing-thawing cycles on acoustic emission characteristics of granite. *Chin. J. Rock Mech. Eng.* **2019**, *38*, 865–874.
18. Su, Z.; Geng, K.; Zhou, F.; Sun, J.; Yu, H. Influence of freeze-thaw cycles on acoustic emission characteristics of granite samples under triaxial compression. *Adv. Civ. Eng.* **2021**, *2021*, 5571680. [[CrossRef](#)]
19. Yang, G.; Liang, B.; Liu, H.; Shen, Y.; Jia, H. Mechanical Properties and Acoustic Emission Characteristics of Thawing Frozen Sandstone. *Adv. Mater. Sci. Eng.* **2022**, *2022*, 2156710. [[CrossRef](#)]
20. Jiang, D.Y.; Zhang, S.L.; Chen, J.; Yang, T.; Wang, X.S.; Xie, K.N.; Jiang, X. Low field NMR and acoustic emission probability density study of freezing and thawing cycles damage for sandstone. *Rock Soil Mech.* **2019**, *40*, 436–444.
21. Xu, J.; Pu, H.; Sha, Z. Experimental Study on the Effect of Brittleness on the Dynamic Mechanical Behaviors of the Coal Measures Sandstone. *Adv. Civ. Eng.* **2021**, *2021*, 6679333. [[CrossRef](#)]
22. Fang, X.; Xu, J.; Wang, P. Compressive failure characteristics of yellow sandstone subjected to the coupling effects of chemical corrosion and repeated freezing and thawing. *Eng. Geol.* **2018**, *233*, 160–171. [[CrossRef](#)]
23. Ding, S.; Jia, H.; Zi, F.; Dong, Y.; Yao, Y. Frost Damage in Tight Sandstone: Experimental Evaluation and Interpretation of Damage Mechanisms. *Materials* **2020**, *13*, 4617. [[CrossRef](#)]
24. Gasc-Barbier, M.; Merrien-Soukatchoff, V. Effect of Freezing-Thawing Cycles on the Elastic Waves’ Properties of Rocks. *Geosciences* **2022**, *12*, 103. [[CrossRef](#)]
25. Wang, L.; Li, N.; Qi, J.; Tian, Y. A study on the physical index change and triaxial compression test of intact hard rock subjected to freeze-thaw cycles. *Cold Reg. Sci. Technol.* **2019**, *160*, 39–47. [[CrossRef](#)]
26. Xu, J.; Pu, H.; Sha, Z. Dynamic Mechanical Behavior of the Frozen Red Sandstone under Coupling of Saturation and Impact Loading. *Appl. Sci.* **2022**, *12*, 7767. [[CrossRef](#)]

27. Chen, T.C.; Yeung, M.R.; Mori, N. Effect of water saturation on deterioration of welded tuff due to freeze-thaw action. *Cold Reg. Sci. Technol.* **2004**, *38*, 127–136. [[CrossRef](#)]
28. Xu, G.; Liu, Q. Freeze-Thaw Cycling and Mechanical Testing Study on Frozen-Thawed Rocks. *Chin. J. Rock Mech. Eng.* **2005**, *24*, 3076–3082.
29. Yamabe, T.; Neaupane, K.M. Determination of some thermo-mechanical properties of Sirahama sandstone under subzero temperature condition. *Int. J. Rock Mech. Min. Sci.* **2001**, *38*, 1029–1034. [[CrossRef](#)]
30. Gao, J.; Xu, C.; Xi, Y.; Fan, L. Degradation of Mechanical Behavior of Sandstone under Freeze-Thaw Conditions with Different Low Temperatures. *Appl. Sci.* **2021**, *11*, 10653. [[CrossRef](#)]
31. Peng, J.; Rong, G.; Cai, M.; Zhou, C.B. A model for characterizing crack closure effect of rocks. *Eng. Geol.* **2015**, *189*, 48–57. [[CrossRef](#)]
32. Li, Y.; Jia, D.; Rui, Z.; Peng, J.; Fu, C.; Zhang, J. Evaluation method of rock brittleness based on statistical constitutive relations for rock damage. *J. Pet. Sci. Eng.* **2017**, *153*, 123–132. [[CrossRef](#)]
33. Zhang, S.; Lai, Y.; Zhang, X. Study on the damage propagation of surrounding rock from a cold-region tunnel under freeze–thaw cycle condition. *Tunn. Undergr. Space Technol.* **2004**, *19*, 295–302. [[CrossRef](#)]
34. Li, X.; Qu, D.; Luo, Y.; Ma, R.; Xu, K.; Wang, G. Damage evolution model of sandstone under coupled chemical solution and freeze-thaw process. *Cold Reg. Sci. Technol.* **2019**, *162*, 88–95. [[CrossRef](#)]
35. Deprez, M.; De Kock, T.; De Schutter, G.; Cnudde, V. A review on freeze-thaw action and weathering of rocks. *Earth Sci. Rev.* **2020**, *203*, 103143. [[CrossRef](#)]
36. Zhang, H.; Yang, G. Research on damage model of rock under coupling action of freeze-thaw and load. *Chin. J. Rock Mech. Eng.* **2010**, *29*, 471–476.
37. Mutlutürk, M.; Altındag, R.; Türk, G. A decay function model for the integrity loss of rock when subjected to recurrent cycles of freezing-thawing and heating-cooling. *Int. J. Rock Mech. Min. Sci.* **2004**, *41*, 237–244. [[CrossRef](#)]
38. Srinivasan, V.; Tripathy, A.; Gupta, T.; Singh, T.N. An Investigation on the Influence of Thermal Damage on the Physical, Mechanical and Acoustic Behavior of Indian Gondwana Shale. *Rock Mech. Rock Eng.* **2020**, *53*, 2865–2885. [[CrossRef](#)]
39. Boyce, G.M.; McCabe, W.M.; Koerner, R.M. *Acoustic Emission Signatures of Various Rock Types in Unconfined Compression*; ASTM International: West Conshohocken, PA, USA, 1981; pp. 142–154.
40. Ranjith, P.G.; Fourar, M.; Pong, S.F.; Chian, W.; Haque, A. Characterisation of fractured rocks under uniaxial loading states. *Int. J. Rock Mech. Min. Sci.* **2004**, *41*, 43–48. [[CrossRef](#)]
41. Sirdesai, N.N.; Gupta, T.; Singh, T.N.; Ranjith, P.G. Studying the acoustic emission response of an Indian monumental sandstone under varying temperatures and strains. *Constr. Build. Mater.* **2018**, *168*, 346–361. [[CrossRef](#)]